Optics Letters

Gyroscopic effect detection in the colliding-pulse hybridly mode-locked erbium-doped all-fiber ring soliton laser

Alexander A. Krylov,[1,*] **Dmitry S. Chernykh,**[2,3] **and Elena D. Obraztsova**[4,5]

[1]*Fiber Optics Research Center of the Russian Academy of Sciences, 119333, 38 Vavilov str., Moscow, Russia*
[2]*Avesta Project Ltd., 142190, 11 Fizicheskaya Str., Laboratory Building, Troitsk, Moscow, Russia*
[3]*P.N. Lebedev Physical Institute of the Russian Academy of Sciences, 119991, 53 Leninskiy Prospekt, Moscow, Russia*
[4]*A.M. Prokhorov General Physics Institute of the Russian Academy of Sciences, 119333, 38 Vavilov str., Moscow, Russia*
[5]*National Research Nuclear University MEPhI (Moscow Engineering Physics Institute), 115409, 31 Kashirskoye shosse, Moscow, Russia*
*Corresponding author: sokolak@mail.ru

We report on the gyroscopic effect detection in the bidirectional ultra-short pulse hybridly mode-locked erbium-doped all-fiber ring soliton laser. Owing to the Kerr nonlinearity contribution through self-phase modulation and self-steepening effects to the carrier-to-envelope phase slip of both clockwise and counterclockwise solitons, wideband controllable tuning of a gyroscope bias point has been demonstrated by means of appropriate adjustment of either intracavity polarization or pump power. Angular velocity detected ranges from 0.12 deg/s to 90 deg/s while rotation sensitivity reaches 7 kHz/(deg/s) for 0.79 m^2 single-coil ring gyroscope in agreement with a calculated scale factor value. The bias point drift responsible for the gyroscope resolution capabilities has been studied on long (during 35-h-long continuous operation experiment) and short (~1 min) time scales.   © 2017 Optical Society of America

Bidirectional mode-locked lasers are promising as highly sensitive intracavity phase interferometric (IPI) sensors of displacement, linear and nonlinear refractive index changes, scattering, and rotation [1,2]. Rotation sensors are of great interest for modern navigation and geodesic systems development that widely use continuous-wave (cw) He–Ne laser gyroscopes nowadays. However, one of the main drawbacks inherent to common cw laser gyroscope is a frequency locking of the counterpropagating waves due to the weak backscattering in the cavity that leads to the dead band origination—the area of angular velocities that a gyroscope cannot measure [3]. Nonetheless, the idea of ultra-short pulse mode-locked laser application for mitigation of this undesirable lock-in effect has been discussed since its origination in the 1960s [4]. As predicted theoretically in [5], if counter-propagating pulses intersect only in two localized points of the ring being away from the backscattering one (e.g., in a vacuum), frequency locking can be suppressed providing dead band narrowing. However, implementation of this idea into practice became possible after colliding-pulse mode-locked (CPML) ultra-short pulse dye ring laser development [6], implying a presence of a saturable absorber (SA) in the cavity for initiating and stabilizing ultra-short pulses (USP) generation in both directions of the ring [7].

Bidirectional operation of a passively mode-locked USP fiber ring laser was realized for the first time only in 2008 by Kieu and Mansuripur [8], 41 years after the first demonstration of the He–Ne bidirectional mode-locked laser by Buholz and Chodorow [4].

Up to now several schemes of bidirectional mode-locked fiber ring lasers have been successfully demonstrated [8–14]. Most of them are mode-locked by carbon nanotube-based (CNT) saturable absorbers and emits conservative solitons.

Though a reliable operation of bidirectional USP mode-locked fiber ring laser was successfully realized, a real gyroscopic effect has not been detected and measured yet. Moreover, few works demonstrate beat-note signal of counterpropagating pulses [8,10,12,15]. As shown in recent work [15], one drawback of reliable gyroscopic effect detection is a dramatic instability of the beat-note frequency stemmed from a huge susceptibility of carrier-to-envelope offset frequencies (f_{ceo}) of counterpropagating pulses to both environmental and intrinsic influence [15–17]. Thus, it is important to elucidate a feasibility of all-fiber USP fiber laser application for a highly reliable dead band free laser gyroscope development that could be a competitive device to the widespread He–Ne laser gyro.

Recently we have presented thoughtful research on the bidirectional erbium-doped all-fiber ring laser hybridly mode-locked with a co-action of a single-walled carbon nanotube-based saturable absorber (SWCNT-SA) and nonlinear polarization evolution introduced through the polarizing fiber (PZ-fiber) implementation [12]. We have obtained a stable beat-note signal of phase-locked clockwise (CW) and

counterclockwise (CCW) pulse trains overlapped outside the cavity. Thus, based on these results we herein extend the gyroscopic effect study.

The principle scheme of the gyroscopic setup consisting of the colliding-pulse hybridly mode-locked (CPHML) erbium-doped fiber soliton laser and external delay line for CW and CCW pulse superposition is depicted in Fig. 1. The detailed information about the CPHML fiber soliton laser is given in Ref. [12].
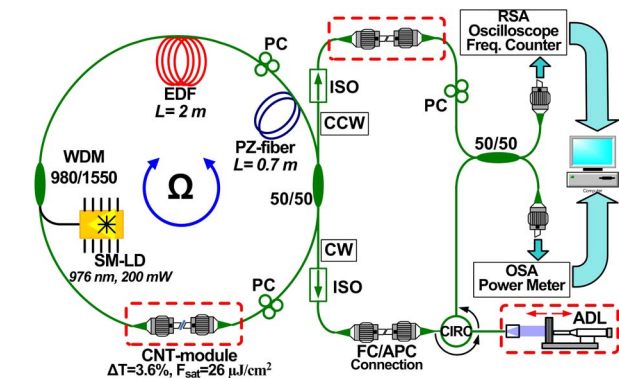
The fiber ring cavity together with a pump diode was put on the plywood disk forming a single-coil gyroscope with a ring diameter of $d \approx 100$ cm. For the sake of thermal stability enhancement, a fiber ring was sealed into thermally isolating material (foam blocks) with carefully prepared channels.

Signals from two ports of the 3-dB coupler were simultaneously analyzed in time and frequency domains by means of the 500-MHz oscilloscope and radio-frequency spectrum analyzer (RSA) with a 300-Hz resolution bandwidth (RBW), respectively. Furthermore, beat-note frequency was filtered out with a low-pass filter and measured with an AGILENT 53132A frequency counter triggered by an external TTL pulse generator [18].
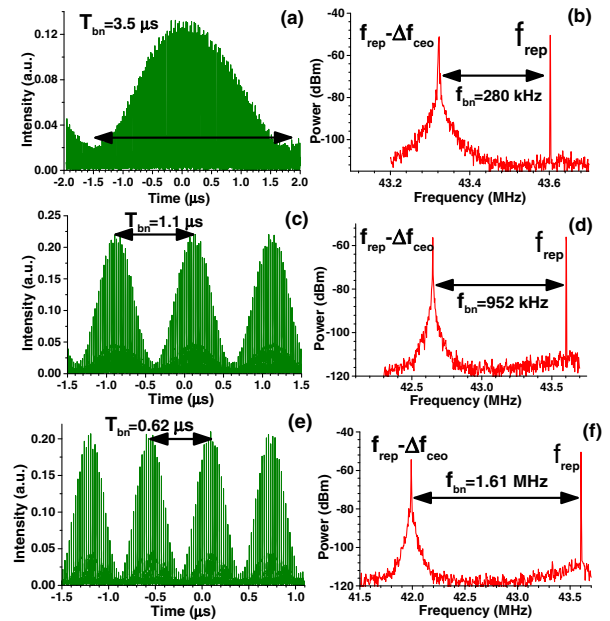
Gyroscopic setup was mounted on the turntable providing a number of discrete angular velocities ranged from 75 deg/h to 360 deg/s to study rotation sensitivity of the gyroscope developed.

Figure 2 demonstrates almost harmonic beat-note signals (a, c, e) having nearly 100% modulation depth, with corresponding beat-note spectra (b, d, f) for strictly different beat-note frequencies of 280 kHz, 952 kHz, and 1.61 MHz in the case of the gyroscope at rest (without rotation). As it follows from Fig. 2, fundamental (repetition rate) frequency peak (f_{rep}) features a high signal-to-noise ratio (more than 70 dB) compared to the beat-note peak (≈ 30 dB); this can be attributed to the beat-note frequency instability (analyzed below), with additional phase and amplitude noise appearing during CW and CCW pulse propagation through an environmentally unstable external delay line.

Worth noting is that beat-note frequency tuning shown in Fig. 2 was realized via polarization state control with a proper PCs adjustment at the constant pump power of 76 mW. Using
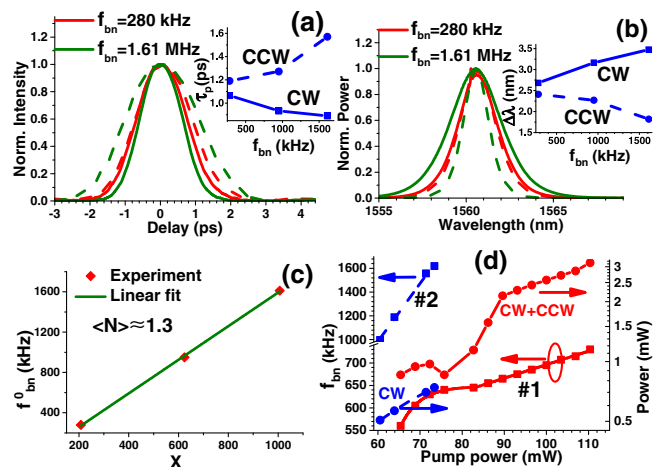

Fig. 2. Beat-note signals (a), (c), (e) and corresponding RF spectra (b), (d), (f) at the constant pump power of 76 mW. RBW = 300 Hz; acquisition time—5 s; $f_{rep} = 43.601$ MHz.

this procedure, beat-note frequency can be continuously tuned between ≈ 60 kHz (beat-notes collapse near dead band area), and ≈ 2.3 MHz with further mode-locking collapse in one of two channels.

To study the evolution of pulse parameters with respect to the beat-note frequency tuning, we have measured CW and CCW pulse-widths (also with spectra FWHM) at the beat-note frequency values taken from Fig. 2. Corresponding autocorrelation traces (ACTs) and pulse spectra at $f_{bn} = 280$ kHz and 1.61 MHz are depicted in Figs. 3(a) and 3(b). Although this measurement was performed only at a few discrete beat-note frequency values owing to experimental capabilities, it is evident that CW and CCW pulse-widths (as well as spectra FWHM)

Fig. 1. Gyroscopic setup. EDF, erbium-doped fiber; SM–LD, single-mode laser diode; ISO, optical isolator; PC, polarization controller; CNT module, single-walled CNT-based thin-film saturable absorber with $\Delta T = 3.6 \pm 0.2\%$ modulation depth of transmission ($T_0 = 58.5\%$) and $F_{sat} = 26$ μJ/cm² saturation fluence [12]; ADL, adjustable delay line; CIRC, fiber circulator.

Fig. 3. ACTs (a) and spectra (b) of CW (solid) and CCW (dashed) pulses upon beat-note frequency variation; f_{bn} dependence on the X parameter (c); f_{bn} also with output average power variation upon pump power tuning (d).

tend to be equalized with beat-note frequency approaching zero. It is a natural trend in the case of soliton generation in the CPHML laser developed, as shown theoretically below.

Since beat-note frequency f_{bn} equals the corresponding difference of CW and CCW carrier-to-envelope offsets Δf_{ceo} [15], it is f_{ceo} dependence on soliton parameters that fully determines f_{bn} tuning shown in Figs. 3(a) and 3(b). Carrier-to-envelope offset frequency f_{ceo} arising from a difference of group and phase velocities of a soliton is defined as follows [1,16,19]:

$$f_{ce} = \frac{\Delta\varphi_{ce}}{2\pi T_{rep}} = f_{rep}\frac{\Delta\varphi_{ce}}{2\pi} = \nu_c\left(1 - \frac{\nu_g(\nu_c)}{\nu_p(\nu_c)}\right). \quad (1)$$

Here ν_g and ν_p are group and phase velocities of a soliton with a carrier frequency ν_c while $\Delta\varphi_{ce}$ is a carrier-to-envelope phase slip of a pulse per pass through the cavity of length L [1,16,19]. According to Ref. [20], $\Delta\varphi_{ce}$ consists of linear $\Delta\varphi_{ce}^L = \beta(\omega_c)L - \omega_c\beta'(\omega_c)$ and nonlinear $\Delta\varphi_{ce}^{NL}$ contributions as:

$$\Delta\varphi_{ce} = \Delta\varphi_{ce}^L + \Delta\varphi_{ce}^{NL} = \beta(\omega_c)L - \omega_c\beta'(\omega_c) - \frac{1}{2}\gamma\frac{E_s}{2\tau_0}L, \quad (2)$$

where β is the linear propagation constant, γ is the fiber nonlinear coefficient (Kerr nonlinearity), and E_s is the energy of a soliton with a pulse-width FWHM of $\tau_s = 2\ln(1 + \sqrt{2})\tau_0$ [20]. As shown in [20,21], $\Delta\varphi_{ce}^{NL}$ arises from the contribution of self-phase modulation (SPM) to the phase velocity (well-known soliton phase) and self-steepening effect (shock term) to the group velocity of a soliton, the latter having 2 times larger effect [20,21]. Thus, beat-note frequency f_{bn} consists of linear f_{bn}^L and nonlinear f_{bn}^{NL} contributions as well, as follows:

$$f_{bn} = \Delta f_{ceo} = (f_{rep}/2\pi)|\Delta\varphi_{ce}^{CW} - \Delta\varphi_{ce}^{CCW}|$$
$$= f_{bn}^L + f_{bn}^{NL} = 2\pi c|D_T|f_{rep}(\Delta\nu^0/\lambda_{CW}) + f_{bn}^{NL}. \quad (3)$$

Here, $D_T \approx -0.11$ ps^2 is total cavity dispersion, and $\Delta\nu^0 = |\nu_{CW}^0 - \nu_{CCW}^0|$ is the carrier frequencies' difference of CW and CCW solitons that is equal to the beat-note frequency: $f_{bn} = |\nu_c^{(1)} - \nu_c^{(2)}|$ [12]. It can be simply estimated that $f_{bn}^L \ll f_{bn}^{NL}$, which means nonlinearity contribution (SPM and self-steepening effects) to the carrier-to-envelope phase slips of CW and CCW pulses to be responsible for the beat-note frequency tuning shown in Figs. 3(a) and 3(b).

According to the above-mentioned analysis and formula (2), beat-note frequency f_{bn} can be expressed as

$$f_{bn} = \Delta f_{ceo} = (f_{rep}/2\pi)|\Delta\varphi_{ce}^{CW} - \Delta\varphi_{ce}^{CCW}| \approx \Delta f_{ceo}^{NL}$$
$$= \frac{f_{rep}L_{res}\gamma}{4\pi}|\langle P_s^{CW}\rangle - \langle P_s^{CCW}\rangle|$$
$$= \frac{f_{rep}L_{res}}{4\pi}\left|\left\langle\frac{1}{L_{NL}^{CW}}\right\rangle - \left\langle\frac{1}{L_{NL}^{CCW}}\right\rangle\right|, \quad (4)$$

where nonlinear length $L_{NL} = (P_s \cdot \gamma)^{-1}$ is introduced for a soliton with an average intracavity power $\langle P_s\rangle = \ln(1 + \sqrt{2}) \cdot \langle E_s\rangle/\langle\tau_s\rangle$. Passing through different segments of the cavity, the soliton undergoes a particular evolution of its characteristics, making it slightly different from a conservative one for which a soliton order $N(N_s = (L_D/L_{NL})^{0.5})$ equals unity ($N = 1$). Introducing the same average soliton order $\langle N\rangle$ for both CW and CCW pulses, Eq. (4) can be rewritten

with regard to the corresponding average soliton pulse-widths τ_s, which are immediately measured in the experiments as

$$f_{bn} = \frac{\langle N^2\rangle f_{rep}L_{res}}{4\pi}\left|\left\langle\frac{1}{L_D^{CW}}\right\rangle - \left\langle\frac{1}{L_D^{CCW}}\right\rangle\right|$$
$$= \frac{(\ln(1 + \sqrt{2}))^2\langle N^2\rangle|D_T|f_{rep}}{\pi}\left|\frac{1}{\langle\tau_{CW}^2\rangle} - \frac{1}{\langle\tau_{CCW}^2\rangle}\right|$$
$$= X \cdot \langle N^2\rangle. \quad (5)$$

The dependence of the beat-note frequency f_{bn} on the dimensionless value X for experimental parameters taken from Fig. 3(a) is plotted on Fig. 3(c). The high-quality linear fit of experimental data gives the slope $B = \langle N^2\rangle = 1.668 \pm 0.008$, yielding the average intracavity order $\langle N\rangle \approx 1.3$ for CW and CCW solitons of sensible value.
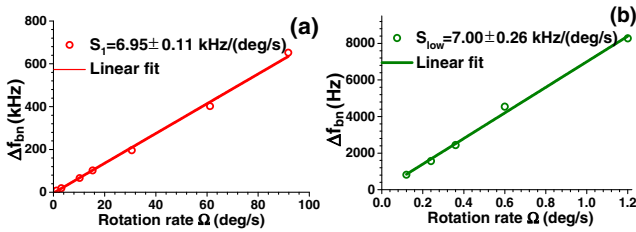
Further, we have studied beat-note frequency dependence on the laser pump power P_{pump} that is demonstrated in Fig. 3(d) (PCs were not adjusted in this experiment) for two different initial operation points [designated as #1 (solid lines) and #2 (dashed lines)] set with appropriate PCs adjustments. As seen, pump power increases results in the beat-note frequency growth in both cases. Moreover, f_{bn} evolution of point #1 consists of two different stages exhibiting saturation and linear behavior having a slope of $df_{bn}/dP_{pump} = d(\Delta f_{ceo})/dP_{pump} = 3.00 \pm 0.05$(kHz/mW), which is ~3 orders of magnitude less than df_{ceo}/dP_{pump} for a common soliton fiber laser [22]. The evolution of point #2 is linear over acceptable P_{pump} tuning range with a corresponding slope of $d(\Delta f_{ceo})/dP_{pump} = 49 \pm 2$(kHz/mW).

Thus, we attribute behavior observed to the particular set of the initial operation points for CW and CCW channels by means of the appropriate PCs adjustments.
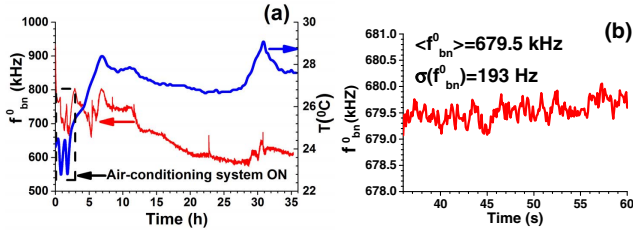
The saturation segment of f_{bn} dependence for point #1 obviously correlates with corresponding nonlinear behavior of $P_{CW} + P_{CCW}$ dependence. It should be noted that output average power reduction with pump power growth can be associated with loss increase inside the laser cavity; this can be originated in this case of the nonlinear polarization evolution (NPE) overdriving for single or both channels from the particular set of the initial operation points for CW and CCW channels as well.

During a turntable rotation we have detected the gyroscopic effect registered as a beat-note frequency shift with respect to the bias frequency f_{bn}^0 (for a gyroscope at rest). Thus, the gyroscopic effect in the rotating a USP ring laser can be interpreted as shifts of CW and CCW combs in opposite directions in the frequency domain. Measured rotation sensitivity plots ($f_{bn}^0 \approx 700$ kHz) are shown in Fig. 4 (beat-note frequency shifts were averaged for the same CW and CCW rotation rates Ω of the turntable). Meanwhile, total rotation sensitivity is depicted in Fig. 4(a), while Fig. 4(b) demonstrates rotation sensitivity for low angular velocities only. The highest angular velocity detected is $\Omega_{max} = 90$ deg/s, while the lowest one of $\Omega_{min} = 0.12$ deg/s $= 432$ deg/h results from the f_{bn}^0 instability that will be further analyzed.

High-quality linear approximation of experimental data from Fig. 4(a) yields overall rotation sensitivity of $S_1 = (6.95 \pm 0.11)$ kHz/(deg/s) and $S_1^{low} = (7.00 \pm 0.26)$ kHz/(deg/s)–rotation sensitivity for low angular velocities derived from Fig. 4(b). Herewith, well-known rotation sensitivity of an ideal single-coil ring laser gyroscope (far from the dead band) is expressed as follows:

Fig. 4. Rotation sensitivity measurements. (a) Total; (b) low rotation rates.

Fig. 5. (a) Long-term and (b) short-term f_{bn}^0 stability measurements.

$$\Delta f_{bn}[Hz] = (4A/\lambda_0 nP)\Omega[rad/s] = S \cdot \Omega,$$

$$S = 4A/\lambda_0 nP = (d/\lambda_0 n)(\pi/180)[Hz/\deg/s]. \quad (6)$$

Here, $P = \pi d$ is a gyroscope perimeter (circle length); λ_0 is a carrier wavelength in vacuum ($\lambda_0 \approx 1.56$ μm); and n is a refractive index of laser media, e.g., silica glass ($n \approx 1.46$). Taking into account above-mentioned experimental parameters, the calculated scale factor is $S_1 = 7.66$ kHz/(deg /s) in good agreement with the measured rotation sensitivity value. Moreover, we have undoubtedly proved the inverse dependence of rotation sensitivity S on refractive index n of the laser media [23].

Finally, we have studied both short-term and long-term stability of the gyroscope bias frequency by means of recording f_{bn}^0 evolution during continuous operation of the CPHML laser at rest. Figure 5(a) demonstrates ≈35 – h – long f_{bn}^0 evolution in the case of the laser pump power of 72 mW (frequency counter gate time $\tau_g = 100$ ms; dead time $-\tau_d \approx 4.4$ ms) with simultaneous record of the temperature (every 15 min) near the gyroscopic setup. After turning on the laser, f_{bn}^0 exhibits exponentially decaying behavior with a time constant of 4.5 min followed by a stochastic drift with both slow (due to temperature variations) and fast (due to vibrations and pump power instability) fluctuations. There is evident correlation between temperature evolution and f_{bn}^0 drift as seen on Fig. 5(a) proving a contribution of thermal processes to the slow variations in f_{bn}^0. Nonetheless, f_{bn}^0 evolution on the short time scale (of ~40 sec) presented in Fig. 5(b) demonstrates as small as $\sigma(f_{bn}^0) = 193$ Hz standard deviation (and $\sigma(f_{bn}^0)/\langle f_{bn}^0\rangle \approx 3 \times 10^{-4}$) that expects gyroscope resolution (the smallest detectable change in rotation velocity) of

$R \sim \sigma(f_{bn}^0)/S_1 = 0.028$ deg /s $= 100$ deg /h. Unfortunately, this value is far beyond the required resolution (~0.01 deg /h) of laser gyros applicable for navigation purposes [3,10].

Based on our experimental results we claim noticeable bias frequency drift closely related to the problem of the carrier-to-envelope offset frequency stability [16,17] to be the key drawback for realization of a highly sensitive gyroscope based on the bidirectional USP all-fiber ring laser.

In summary, we have detected and measured, for the first time to the best of our knowledge, a real gyroscopic effect in the rotating colliding-pulse hybridly mode-locked erbium-doped all-fiber ring soliton laser emitting stable pico- and femtosecond pulses in both directions of the ring.

REFERENCES

1. L. Arissian and J.-C. Diels, Laser Photon. Rev. **8**, 799 (2014).
2. S. Diddams, B. Atherton, and J.-C. Diels, Appl. Phys. B **63**, 473 (1996).
3. W. W. Chow, J. Gea-Banacloche, L. M. Pedrotti, V. E. Sanders, W. Schleich, and M. O. Scully, Rev. Mod. Phys. **57**, 61 (1985).
4. N. Buholz and M. Chodorow, IEEE J. Quantum Electron. **3**, 454 (1967).
5. J. Chesnoy, Opt. Lett. **14**, 990 (1989).
6. D. Gnass, N. P. Ernsting, and F. P. Sehifer, Appl. Phys. B **53**, 119 (1991).
7. R. L. Fork, B. I. Greene, and C. V. Shank, Appl. Phys. Lett. **38**, 671 (1981).
8. K. Kieu and M. Mansuripur, Opt. Lett. **33**, 64 (2008).
9. X. Zhao, Z. Zheng, Y. Liu, G. Hu, and J. Liu, IEEE Photon. Technol. Lett. **26**, 1722 (2014).
10. A. Braga, J.-C. Diels, R. Jain, R. Kay, and L. Wang, Opt. Lett. **35**, 2648 (2010).
11. C. Zeng, X. Liu, and L. Yun, Opt. Express **21**, 18937 (2013).
12. A. A. Krylov, D. S. Chernykh, N. R. Arutyunyan, V. V. Grebenyukov, A. S. Pozharov, and E. D. Obraztsova, Appl. Opt. **55**, 4201 (2016).
13. M. Chernysheva, M. Al Araimi, H. Kbashi, R. Arif, S. V. Sergeyev, and A. Rozhin, Opt. Express **24**, 15721 (2016).
14. X. Yao, Appl. Opt. **53**, 27 (2014).
15. R. Gowda, N. Nguyen, J.-C. Diels, R. A. Norwood, N. Peyghambarian, and K. Kieu, Opt. Lett. **40**, 2033 (2015).
16. N. R. Newbury and W. C. Swann, J. Opt. Soc. Am. B **24**, 1756 (2007).
17. J. Kim and Y. Song, Adv. Opt. Photon. **8**, 465 (2016).
18. S. T. Dawkins, J. J. McFerran, and A. N. Luiten, IEEE Trans. Ultrason. Ferroelectr. Freq. Control **54**, 918 (2007).
19. L. Matos, O. D. Mucke, J. Chen, and F. X. Kartner, Opt. Express **14**, 2497 (2006).
20. H. A. Haus and E. P. Ippen, Opt. Lett. **26**, 1654 (2001).
21. M. J. Ablowitz, B. Ilan, and S. T. Cundiff, Opt. Lett. **29**, 1808 (2004).
22. B. R. Washburn, W. C. Swann, and N. R. Newbury, Opt. Express **13**, 10622 (2005).
23. S. Sunada, S. Tamura, K. Inagaki, and T. Harayama, Phys. Rev. A **78**, 053822 (2008).